CASPT2//CASSCF and TDDFT//CASSCF Mapping of the Excited State Isomerization Path of a Minimal Model of the Retinal Chromophore

Simona Fantacci,[†] Annapaola Migani,[‡] and Massimo Olivucci*[,‡,§]

Istituto CNR di Scienze e Tecnologie Molecolari (ISTM), c/o Dipartimento di Chimica, Università degli Studi di Perugia, via Elce di Sotto 8, Perugia, I-06123 Italy, Dipartimento di Chimica, Università di Siena, via Aldo Moro, Siena, I-53100 Italy, and Centro per lo Studio dei Sistemi Complessi, Università di Siena, via Pendola 37, Siena, I-53100 Italy

Received: July 30, 2003; In Final Form: November 7, 2003

In this work we explore the validity of the application of TDDFT methods to the study of excited state reactivity problems. Accordingly, TDDFT//CASSCF calculations have been used to evaluate the excited state isomerization path of a retinal chromophore model and have been compared with the path obtained at the more expensive CASPT2//CASSCF level. We show that the TDDFT and CASPT2 excited state energy profiles are qualitatively similar. Indeed, remarkably, the TDDFT//CASSCF strategy achieves a qualitatively correct description of the intersection region, which is a basic mechanistic feature of photochemical processes. Quantitative differences are found in the region of the energy profile characterized by a coupled stretching−twisting deformation. This discrepancy reflects the difference in the equilibrium values of the bond lengths of the planar excited state structures when evaluated at the TDDFT and CASPT2 levels. We stress that our results support the use of TDDFT for the evaluation of energy profiles along CASSCF reaction coordinates. Thus, in no way shall such results be considered as indicative of the validity of TDDFT for the calculation of excited state equilibrium structures or reaction coordinates.

1. Introduction

Presently, there is a broad interest in assessing the performance of quantum chemical methodologies for predicting excited state properties such as excited state equilibrium geometries and spectral parameters (e.g., absorption and emission maxima). The relatively recent discovery that low-lying potential energy surface crossing points such as conical intersections[1] are substantially ubiquitous in organic and bioorganic compounds further motivates the work in the field. In fact, the need to include a quantitative description of these features in the mechanistic scenario of observed photochemical or photophysical events calls for a balanced and accurate description of ground and excited states.

The use of quantum chemical methods that include the effects of dynamic electron correlation (e.g., multireference configuration interaction or multireference second-order perturbation theory) is mandatory for a satisfactory evaluation of the energy gap between different electronic states.[2−5] Thus, a considerable amount of work on the photochemistry and photophysics of medium-size organic compounds has been carried out by using mixed computational strategies such as the one based on the CASPT2//CASSCF level of theory.[6,7] At this level the (ground or excited state) equilibrium structure of the molecule is determined via CASSCF geometry optimization. However, the potential energy is evaluated by a single-point CASPT2 calculation to allow for the treatment of the dynamic electron correlation.

This CASPT2//CASSCF strategy not only allows for the computation of excited state stationary points but also allows for the mapping of entire excited state relaxation or reaction paths. In this case the full reaction coordinate is computed (e.g., by using the IRD or IRC methods[8,9]) at the CASSCF level while the corresponding energy profile is computed at the CASPT2 level.

In different applications[6,10−12] it has been shown that it is reasonable to apply CASPT2 corrections to CASSCF potential energy profiles to incorporate dynamic correlation effects. It should be pointed out that the photochemical scenario/mechanism is preserved after the CASPT2 correction. However, this is not always the case. In a recent contribution on the ultrafast decay of singlet excited cytosine,[13] it was shown that in the presence of nearly degenerate excited states (e.g., $\pi-\pi^*$ and n$-\pi^*$ or two close $\pi-\pi^*$'s) the CASPT2 method yields a photochemical scenario different from that obtained at the CASSCF level. However, notice that, in the test case selected for this paper, there are no nearly degenerate excited states as reported in ref 14.

The recent implementation of CASPT2 numerical first derivatives[15] has allowed for the direct comparison of CASPT2//CASSCF and CASPT2//CASPT2 ground state reaction paths for the C−N σ-bond breaking process in the CH_3–N_2 radical, i.e., a reactant small enough to allow for expensive CASPT2 optimizations. The results show that, in this case, the CASPT2//CASSCF and CASPT2//CASPT2 reaction coordinates and energy profiles are virtually coincident.[15]

While the CASPT2//CASSCF strategy offers a computational tool for the evaluation of excited state parameters and reaction paths, its routine use is restrained by at least two factors: the high computational cost and the choice of the active space. The second factor is particularly important as, ideally, the active space must comprise all the occupied and empty orbitals that could possibly be involved in the electronic excitation or change

* To whom correspondence should be addressed.
[†] Istituto CNR di Scienze e Tecnologie Molecolari (ISTM), c/o Dipartimento di Chimica, Università degli Studi di Perugia.
[‡] Dipartimento di Chimica, Università di Siena.
[§] Centro per lo Studio dei Sistemi Complessi, Università di Siena.

10.1021/jp0362335 CCC: $27.50
Published on Web 01/27/2004

in bonding that one wishes to describe. In practice, an active space comprising 12 electrons and 12 orbitals represents (for asymmetric molecules) the current practical limit. This is particularly frustrating for top applications in photobiology that often require the treatment of large conjugated or aromatic chromophores containing extended π-systems, and becomes prohibitive for complex systems containing transition metals. The development of time-dependent density functional theory (TDDFT) methods[16,17] raises much interest as, in certain cases, these methods may provide a solution to the computational cost and active space size problem mentioned above.

In principle, it is known that TDDFT methods can be applied to excited states that can be described within the linear response theory.[16,17] Notably, the low-lying excited states of different classes of organic chromophores are dominated by single excitations and are substantially single-reference problems. In these cases TDDFT has been shown to provide a valid alternative to conventional quantum chemical methods. In particular, the recent work of Furche et al.[18] shows, through the analysis of an extensive series of benchmark molecules going from BeH to benzene, that high-quality excited state geometric as well as spectroscopic parameters can be computed via TDDFT. Moreover, for a series of *trans*-polyene oligomers (from butadiene to decapentaene), it has been demonstrated that TDDFT accurately describes transition energies with a substantial double excitation character.[19] Also, a recent spin-flip approach within TDDFT theory has allowed reliable description of bond breaking in ethylene and equilibrium properties of diradicals.[20] Notably, TDDFT methods have been recently shown to quantitatively reproduce the UV−vis spectral features of large transition metal complexes in solution, in terms of band separation, relative band intensities, and solvatochromic shifts,[21,22] expanding the applicability of TDDFT methods to complex metallorganic systems in the condensed phase.

Despite this progress, little testing of TDDFT methods for excited state reactivity problems has been reported. In its simpler form such testing must involve the evaluation of energy profiles along mapped excited state reaction paths. In other words, one wants to see if single-point TDDFT calculations can successfully allow for the treatment of the dynamic electron correlation as an alternative to the more expensive CASPT2 treatment. For this reason, in the present work, we present a detailed comparison of a CASPT2//CASSCF and a TDDFT//CASSCF reinvestigation of the excited state (S_1) isomerization path of the *Z*-penta-2,4-dieniminium cation **1** (a minimal model of the 11-*cis*-retinal protonated Schiff base chromophore of the visual receptor rhodopsin).[23] We stress that the CASPT2//CASSCF approach has been previously validated to describe the photoisomerization path of a realistic (five double bonds) retinal chromophore model.[6]

The TDDFT//CASSCF S_1 vertical excitation energy of a five double bond retinal model has been tested against CASSCF and has been shown to reproduce the target CASSCF value with an error of 17%.[24] The large error should not be surprising because CASSCF does not include dynamic correlation, in contrast to TDDFT.

A TDDFT//CASSCF versus CASPT2//CASSCF comparative study has been previously reported for the intramolecular proton transfer of $^1(\pi-\pi^*)$ *o*-hydroxybenzaldehyde.[25] In the present work we focus on a reaction of different nature (a Z/E photoisomerization). In contrast to the previously reported work, the reaction path is computed as a minimum energy path (MEP) in mass-weighted coordinates[8] and with no symmetry constraints. Furthermore, the path is followed up to the region of intersection between the S_0 and S_1 energy surfaces.

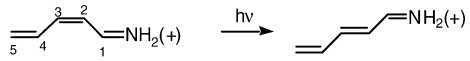

1

In previous work[14] we have provided evidence that the S_1 state of **1** has a dominating singly excited (hole pair) character that is maintained all along the reaction coordinate. For this reason, we believe that this cation represents an ideal candidate for testing TDDFT as the description of the excited state should be possible within the linear response theory.

The excited state isomerization path of **1** (see Scheme 1) connects its planar Franck−Condon (FC) structure to a 66° [26] twisted S_1/S_0 conical intersection (CI) that provides a channel for efficient return to the ground state (S_0). The geometric progression associated with this change is not straightforward, but it is sequentially dominated by two different modes: a stretching and a twisting mode, respectively. In particular, the initial relaxation connects FC to a planar structure FS. At the CASSCF level of theory (i.e., when the dynamic correlation contribution is not considered), FS[27] is unstable with respect to twisting deformation about the central C_2-C_3 bond and thus this structure evolves along a barrierless path toward CI. In our view two features of the reaction coordinate described above allow for an unprecedented testing of the CASPT2 and TDDFT levels when used to account for the dynamic electron correlation effects: (i) the bimodal character along the coordinate provides the opportunity to test the effect of the dynamic electron correlation energy along two different types of chemically relevant molecular deformations, and (ii) the fact that the coordinate terminates at a conical intersection allows for a direct

SCHEME 1

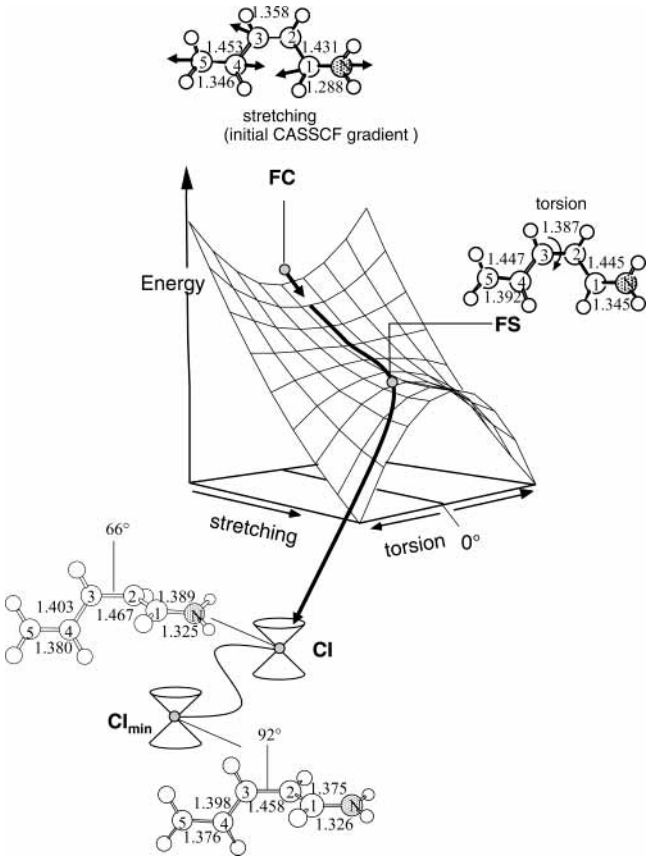

test of the ability of TDDFT to describe regions of crossing between the ground state and a singly excited (hole-pair) state.

Below we show that while the CASPT2//CASSCF and TDDFT//CASSCF treatments give the same value for the vertical excitation energy of **1**, quantitative differences between the two treatments are found along the reaction coordinate segment dominated by the coupled stretching−twisting mode. Despite this discrepancy, the TDDFT//CASSCF energy profile is found to correctly approach the conical intersection region.

2. Computational Methods

The photoisomerization path of the retinal model **1** has been computed using fully unconstrained ab initio quantum chemical computations in the framework of the CASPT2//CASSCF strategy.[6,7] This requires that the reaction coordinate be computed at the complete active space self-consistent field (CASSCF) level of theory and that the corresponding energy profile is reevaluated at the multiconfigurational second-order Møller−Plesset perturbation theory level (here we use the CASPT2 method implemented in MOLCAS-5[28]) to take into account the effect of electron dynamic correlation. More specifically, the CASSCF S_1 excited state minimum energy path (MEP) reaction coordinate data of **1** are from ref 23 and were performed using the 6-31G* basis set and an active space of six electrons in six orbitals (6e/6o).The single-point CASPT2 computations were performed along a selected number of MEP points using a two-root (S_1, S_0) state-average (0.5, 0.5) CASSCF zero-order wave function with a 6e/6o complete active space and the 6-31G* basis set.

Vertical excitation energies at selected CASSCF geometries along the reaction pathway have been computed by means of TDDFT methods using the same 6-31G* basis set employed in the CASSCF and CASPT2 calculations and investigating basis set expansion. We also optimized the ground state geometry of the retinal model **1** using the considered exchange-correlation (XC) functionals (see below).

To check the dependence of our results on the choice of the particular XC functional employed, we used the BPW91 and PBE functionals and the B3LYP and PBE0 functionals, as representative of pure generalized gradient approximation (GGA) and hybrid XC functionals, respectively.

The BPW91 and B3LYP XC functionals are very popular in quantum chemistry and have been largely applied, while the PBE and PBE0 XC functionals have been more recently developed and shown to give accurate vertical excitation energies over a broad range of excited states.[29,30] In the BPW91 functional the Becke exchange[31] is combined with the Perdew−Wang correlation.[32] In the B3LYP functional, the exchange part B3 is the hybrid method proposed by Becke[33] that includes a weighted sum of Slater functionals,[34] Becke's 1988 gradient correction,[31] and Hartree−Fock (HF) exchange. Its correlation part is also a weighted sum of two terms, the Vosko−Wilk−Nusair (VWN)[35] and the gradient-corrected Lee−Yang−Parr (LYP) correlation functionals.[36,37]

In PBE the XC functional is defined according to the Perdew, Burke, and Ernzerhof parametrization.[38,39] The PBE0 functional results from adding to the PBE XC functional a fixed amount of HF exchange, according to the formula $(1/4)(E_X^{HF} - E_X^{PBE})$.[29,30,40]

To investigate the effect of the basis set on the vertical excitation energies, single-point TDDFT calculations have been repeated on the optimized CASSCF/6-31G* ground state structure of system **1**, with the 6-311+G* and 6-311++G(3df,3pd) basis sets, using all the considered XC functionals.

TABLE 1: Optimized Bond Lengths of Retinal Model 1 at Different Levels of Theory, CASSCF, CASPT2, B3LYP, PBE0, BPW91, and PBE

	C_1-N	C_1-C_2	C_2-C_3	C_3-C_4	C_4-C_5
CASSCF/6-31G*[a]	1.288	1.431	1.358	1.454	1.346
CASPT2/6-31G*[b,c]	1.311	1.411	1.375	1.435	1.354
B3LYP/6-31G*	1.315	1.408	1.379	1.434	1.351
PBE0/6-31G*	1.308	1.406	1.374	1.431	1.348
BPW91/6-31G*	1.324	1.412	1.389	1.435	1.362
PBE/6-31G*	1.323	1.411	1.388	1.434	1.361
CASPT2/6-31G*[b,d]	1.356	1.428	1.419	1.424	1.385

[a] Data from refs 14 and 23. [b] Data from ref 15. Note that the bond distances for the ground state geometry of **1** computed at the CASSCF/6-31G* level of theory reported in Table 9 of ref 15 are not correct. [c] Ground state optimized structure at the CASPT2 level. [d] First electronically excited state optimized structure at the CASPT2 level.

The 6311+G* basis set was also employed to recompute the CASPT2 vertical excitation energy at the optimized CASSCF/6-31G* ground state minimum.

We will hereafter indicate by BSI, BSII, and BSIII the 6-31G*, 6-311+G*, and 6-311++G(3df,3pd) basis sets, respectively. The relatively small computational overhead of TDDFT with respect to CASPT2 allows us to investigate basis set convergence up to BSIII, which comprises a total of 516 primitive Gaussians, contracted to 378 basis functions.

All the DFT/TDDFT calculations were performed using the Gaussian 98 package.[41,42]

3. Results and Discussion

3.1. Optimized Geometry of 1 and Relative Vertical Excitation Energy. To check the consistency of the ground state properties obtained at different levels of theory, we optimized the retinal model **1** using all four different functionals with BSI. Optimized bond lengths are reported in Table 1.

As can be noticed, the agreement between DFT and CASSCF geometric parameters is good, with the DFT results featuring the same bond alternate pattern exhibited by the CASSCF geometry, even though, as also discussed in ref 24, the DFT optimized structures slightly favor an overall more delocalized geometry. Furthermore, notice that the ground state geometries computed at the B3LYP and PBE0 levels of theory are essentially identical to the corresponding CASPT2 optimized geometry,[15] with pure GGA functionals slightly overestimating C−N bond distances.

To disentangle effects due to the basis set and to the use of different XC functionals, we computed the S_1 vertical excitation energy at the CASSCF geometry, using the BSI, BSII, and BSIII and all the XC functionals. The results are reported in Table 2, together with the vertical excitation energies obtained with BSI at the corresponding DFT optimized geometry for a direct comparison. Notably, TDDFT vertical excitation energies computed on the relative DFT optimized geometries do not show significant variations with respect to those computed at the CASSCF optimized geometry, with an overall increase close to 1 kcal mol^{-1} (see Table 2) reflecting the geometric differences between DFT and CASSCF.

It is worth noting that, with BSI, both hybrid and pure XC functionals provide good estimates of the vertical excitation energy at the CASSCF ground state equilibrium geometry, with differences falling in the range +1.3 to +6.7 kcal mol^{-1} with respect to the CASPT2//CASSCF result; see Table 2. Interestingly, an overall better agreement is computed with pure BPW91 and PBE XC functionals, which quantitatively reproduce the CASPT2//CASSCF value, with a negligible overestimate of the

TABLE 2: Vertical Excitation Energies (kcal mol^{-1}, eV in Parentheses) Computed at Different Levels of Theory, CASPT2//CASSCF, CASPT2//CASPT2, TDDFT//DFT, and TDDFT//CASSCF, and with Different Basis Sets

optim	B3LYP			PBE0			BPW91			PBE			CASPT2	
geom	BSI	BSII	BSIII	BSI	BSII	BSIII	BSI	BSII	BSIII	BSI	BSII	BSIII	BSI	BSII
CASSCF (BSI)	97.89 (4.24)	95.67 (4.15)	94.89 (4.11)	99.35 (4.31)	97.38 (4.22)	96.59 (4.19)	93.97 (4.07)	91.97 (3.99)	91.20 (3.95)	94.01 (4.08)	91.81 (3.98)	91.02 (3.95)	92.69 (4.02)	89.40 (3.88)
DFT (BSI)	98.65 (4.28)			100.44 (4.36)			95.16 (4.13)			95.30 (4.13)			111.14[a] (4.82)[a]	
CASPT2 (BSI)													90.42 (3.92)	

[a] CASSCF S_1 vertical energy (kcal mol^{-1}, eV in parentheses) from ref 23.

vertical excitation energy of only +1.3 kcal mol^{-1}. This trend is in agreement with previous studies showing that the GGA functionals provide lower excitation energies than hybrid functionals, probably because of the smaller HOMO−LUMO gap produced by the GGA functionals.[30,43]

In any case, all the TDDFT vertical excitation energies are in considerably better agreement with the CASPT2//CASSCF value than the corresponding CASSCF//CASSCF estimate, which is blue-shifted by 18.5 kcal mol^{-1} relative to the CASPT2//CASSCF energy. This shift of the vertical excitation energies reflects the effect of including dynamic electron correlation, which preferentially stabilizes the singly excited state with respect to the ground state.

With BSII the differences between the two methods fall in the range +2.4 to +8.0 kcal mol^{-1}, with the pure GGA functionals still providing a slightly better agreement. Thus, comparison of the TDDFT and CASPT2 results obtained with BSI and BSII suggests that the increase in size of the basis set leads to a slightly larger discrepancy between the two methods. It is also worth noting that the TDDFT//CASSCF S_1 vertical excitation energies are almost converged with respect to basis set expansion. The TDDFT energies are stabilized by about 2 kcal mol^{-1} as the basis set increases from BSI to BSII and by only ca. 0.8 kcal mol^{-1} from BSII to BSIII. A similar trend is seen in the CASPT2//CASSCF energy that is also stabilized by ca. 3 kcal mol^{-1} upon increasing the basis set size from BSI to BSII.

Although a direct comparison of the computed λ_{max} values with the experimental data is not possible for **1**, the CASPT2//CASSCF vertical excitation energies computed for a more realistic retinal model[6] are consistent with the λ_{max} values observed for the *N*-butylamine retinal protonated Schiff base in solution, suggesting that the TDDFT vertical excitation energies are reliable to a similar extent.

As a last point, we wish to compare the TDDFT//DFT vertical excitation energies obtained with hybrid functionals to the CASPT2//CASPT2 value since the DFT−B3LYP (DFT−PBE0) and CASPT2 geometries are almost coincident (see Table 1). We observe that, despite the similarity between the ground state optimized geometries, the TDDFT−B3LYP and TDDFT−PBE0 methods both overestimate the excitation energy by 8.23 and 10.02 kcal mol^{-1}, respectively. Therefore, these data further confirm the idea, already reported above, that the GGA functionals provide a better agreement with the CASPT2//CASPT2 value than the hybrid functional.

3.2. Energy Profiles. All CASSCF//CASSCF, CASPT2//CASSCF, and TDDFT//CASSCF S_1 and S_0 energy profiles are collected in Figure 1. The first energy profile has already been reported in ref 23.

As can be noticed, at the CASPT2 level the S_1 curve shows a local minimum configuration, hereafter defined as FS′, located 7.1 kcal mol^{-1} below FC, and an energy barrier of 2.5 kcal mol^{-1} located in correspondence with a 9° twisted structure.

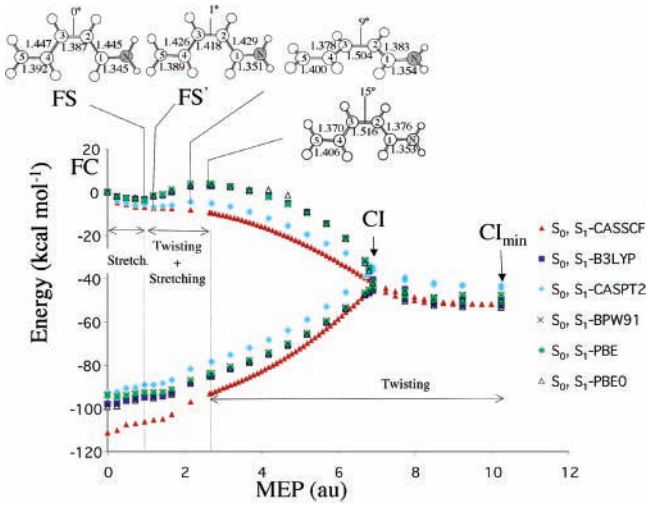

Figure 1. Energy profiles along the S_1 photoisomerization coordinate of **1** at CASPT2//CASSCF and TDDFT//CASSCF levels of theory. The FS and FS′ structures (geometric parameters in angstroms and degrees) correspond to the local minimum along the TDDFT and CASPT2 curves, respectively. The local maximum is located in correspondence to a 15° twisted geometry along the TDDFT lines and a 9° twisted geometry along the CASPT2 profile.

Notice that the structure FS′ defining the local energy minimum along the CASPT2//CASSCF profile is very similar to the CASPT2 S_1 optimized structure[15] (see Table 1) with differences in bond lengths below 0.005 Å.

As the system initiates to relax toward FS, the CASPT2 and TDDFT energy profiles begin to diverge, with the S_1 TDDFT curve being ca. 2−3 kcal mol^{-1} above the CASPT2 one and yielding a less stabilized minimum in correspondence with the FS geometry. However, the S_1 TDDFT energy profile in this region qualitatively reproduces the CASPT2 curve, correctly showing the presence of a minimum located 2.8−3.7 kcal mol^{-1} below FC and of an energy barrier 6.3−7.7 kcal mol $^{-1}$ above the minimum, although shifted to a structure with a 15° twisting. The depth of the TDDFT minimum and the height of the barrier do not depend on the choice of the XC functional, see Table 3, or on the basis set used (results not shown).

Notably, a slight deviation between the CASPT2 and DFT energy profiles is observed also for the S_0 state, with the DFT curve constantly stabilized by 3−5 kcal mol^{-1}.

Notice that in realistic retinal models FS′ would correspond to the experimentally observable transient fluorescent state whose emission maximum has been correctly predicted at the CASPT2//CASSCF level.[6] It is therefore apparent that the TDDFT//CASSCF level would predict an emission maximum blue-shifted (6.9−10.6 kcal mol^{-1}), depending on the XC functional with respect to the CASPT2 value, taking into account the deviation from both the S_0 and S_1 states. Also in this case the GGA functionals give a smaller deviation with respect to

TABLE 3: S_1 Minimum Depth (kcal mol^{-1}), S_1 Barrier Height (kcal mol^{-1}), and S_1-S_0 Gap at the Minimum (kcal mol^{-1}, eV in Parentheses)

	CASSCF	CASPT2	B3LYP	PBE0	BPW91	PBE
min[a]	no	−7.07	−3.36	−2.84	−3.72	−3.63
max[b]	no	2.49	6.27	6.16	7.54	7.75
$\Delta E(S_1-S_0)$	97.90	81.98	91.53	92.63	88.91	88.94
	(4.25)	(3.55)	(3.97)	(4.02)	(3.86)	(3.86)

[a] Relative to FC. [b] Relative to the S_1 minimum.

the CASPT2 reference value than the hybrid functionals. A similar tendency to overestimate the fluorescence maximum by TDDFT//CASSCF relative to CASPT2//CASSCF has been reported in excited state intramolecular proton transfer systems.[25]

From inspection of Figure 1, it is evident that the discrepancy between CASPT2 and TDDFT increases in the reaction coordinate region dominated by coupled stretching−twisting deformations (see Scheme 1 and the discussion in section 1). Indeed, beyond the observed barrier, the TDDFT and CASPT2 S_1 energy profiles are qualitatively similar and, remarkably, the corresponding S_1-S_0 energy gap correctly decreases up to the CI point, where it reaches its minimum values. Nevertheless, the TDDFT S_1-S_0 difference is constantly higher than that computed at the CASPT2 level. To gain some insight into the origin of such a CASPT2−TDDFT discrepancy, it is interesting to analyze the 15° twisted structure defining the top of the TDDFT barrier. This structure displays, with respect to the initial structure FC (see Scheme 1), the maximum stretching expansion. In other words, upon S_1 relaxation the double bonds expand and the single bonds contract up to the 15° twisted structure where this stretching deformation reaches its maximum value. In fact, beyond the barrier the reaction coordinate is essentially dominated by the twisting about the central bond (C_2-C_3) with only a limited contribution in the stretching that slightly contracts back before reaching the CI point. Such a geometric progression indicates that *the major cause of the TDDFT−CASPT2 discrepancy is the coupled stretching−twisting potential*.

Comparison between structures FS′ and FS in Figure 1 shows that at the CASPT2//CASSCF level the excited state equilibrium bond lengths of single and double bonds are, respectively, moderately shorter and larger (i.e., moderately more inverted) than the corresponding TDDFT//CASSCF values. Thus, while the CASPT2 energy profile displays a shallow minimum along the path, the TDDFT profile displays a higher energy barrier and deeper minimum located closer to FC. In contrast, it is apparent that no large differences exist in the CI region, where the TDDFT and CASPT2 curves have similar shapes. This supports the idea that *along the twisting coordinate the TDDFT and CASPT2 treatments yield close descriptions.* In conclusion, the dynamic electron correlation contribution tends to reinforce bond alternation (i.e., stronger double bonds and longer single bonds) in the excited state of protonated Schiff bases, restraining the double-bond/single-bond inversion characterizing the S_1 reaction coordinate (see Scheme 1 and ref 14). This effect is more pronounced at the TDDFT level relative to the CASPT2 level as the TDDFT method favors bond lengths moderately less inverted (i.e., excited state bond lengths displaced toward FC). Such a tendency implies that, at the TDDFT level, the S_1 C_2-C_3 bond maintains part of its original double bond character leading to a stiffer coupled stretching−twisting potential that contributes to the computed barrier.

Recently it has been pointed out that the 66° twisted intersection point CI cannot be isolated but must be one element of an (at least) $(n-2)$-dimensional space (n is the number of vibrational degrees of freedom of the molecule) of conical intersection points called the "intersection space".[23] The lowest lying segment of the intersection space has been mapped out at the CASSCF level of theory. It has been shown that the 66° twisted CI entered by the excited state reaction path is connected along such a branching space segment to a fully (90°) twisted CI_{min} structure (see CASSCF curve in Figure 1). Since the knowledge of the structure of this segment may be relevant for understanding the excited state dynamics, the evaluation of its correct energetics is of interest. In Figure 1 we show that along the CI → CI_{min} region the CASPT2 energy profile is ca. 10 kcal mol^{-1} above the reference CASSCF profile. Nevertheless, the S_0 and S_1 energies remain degenerate all along the segment. Remarkably, all the tested TDDFT levels get a qualitatively acceptable description of the same region. In fact, despite the fact that the degeneracy appears to be slightly lifted (ca. 2 kcal mol^{-1}), the overall description is consistent with the behavior given by both the CASSCF and CASPT2 curves, even though the TDDFT energy profile along the CI → CI_{min} segment of the intersection space is located ca. 10 kcal mol^{-1} lower than the CASPT2 segment.

At the moment we cannot offer a solid theoretical motivation for the apparent success of TDDFT in reproducing, for the case under investigation, the degeneracy region. However, this result is likely to depend on the quality of the description of dynamic electron correlation effects provided by the DFT approach. Indeed, preliminary time-dependent Hartree−Fock (TDHF)// CASSCF calculations fail in describing both the twisting and CI regions of the MEP, suggesting that correlation effects, which are not included in the HF wave function, are relevant for a good description of the reported energy profiles. A detailed analysis of the electronic structure changes along the CASSCF MEP for TDHF and TDDFT methods will be the subject of a forthcoming paper.

4. Conclusions

CASPT2//CASSCF and TDDFT//CASSCF calculations have been performed on the excited state isomerization path of the *Z*-penta-2,4-dieniminium cation, which represents the minimal model of the 11-*cis*-retinal protonated Schiff base chromophore of the visual receptor rhodopsin. The geometry optimization of the model ground state at the DFT level has shown that hybrid functionals provide a structure almost identical to that computed at the CASPT2 level. Moreover, the TDDFT//CASSCF vertical excitation energies computed at the CASSCF equilibrium geometry of the retinal model are in good agreement with those computed at the CASPT2//CASSCF level.

Overall, we have found that, along the excited state reaction coordinate computed at the CASSCF level of theory, the TDDFT excited state energy profile is in qualitative agreement with the CASPT2 results, correctly showing the presence of a local minimum and the related energy barrier. In particular, in the region dominated by the stretching mode, the TDDFT and CASPT2 excited state energy profiles are similar, even though the TDDFT stationary points are characterized by quite different depth and height with respect to those computed at the CASPT2 level.

The differences between the TDDFT and CASPT2 profiles are mainly associated with the region of the reaction coordinate dominated by coupled stretching−twisting deformations. The reason of such a discrepancy probably resides in the fact that the TDDFT methods tend to reinforce the bond alternation in S_1 more than in CASPT2 method. Therefore, at the TDDFT level the S_1 C_2-C_3 bond maintains part of its original double bond character, involving a stiffer coupled stretching−twisting potential which leads to a higher computed barrier. Most remarkably, comparison of the energy profiles demonstrates that the TDDFT//CASSCF method achieves a qualitatively correct description of the intersection region, which is of basic importance for the understanding of the excited state dynamics. We like to stress that our results support the use of TDDFT *for the evaluation of energy profiles along CASSCF reaction coordinates*. Thus, in no way shall such results be considered as indicative of the validity of TDDFT for the calculation of excited state equilibrium structures or reaction coordinates. This more demanding and informative testing would regard the calculation of excited state energy gradients at the TDDFT level. This problem will be addressed in future work.

Acknowledgment. We thank Dr. Filippo De Angelis for helpful discussions. A.P. and M.O. are grateful for an HFSP (RG 0229/2000-M) grant. Funds have been partly provided by the Università di Siena (Progetto di Ateneo 02/04). Part of the required computer time has been provided through a CINECA grant. All the DFT calculations have been performed at ISTM.

References and Notes

(1) Bernardi, F.; Olivucci, M.; Robb, M. A. *Chem. Soc. Rev.* **1996**, 321−328.

(2) Merchán, M.; Serrano-Andrés, L.; Fülscher, M. P.; Roos, B. O. In *Recent Advances in Multireference Methods*; Hirao, K., Ed.; World Scientific Publishing Company: Amsterdam, The Netherlands, 1998.

(3) Roos, B. O.; Fülscher, M. P.; Malmqvist, P.-Å.; Merchán, M.; Serrano-Andrés, L. In *Quantun Mechanical Electronic Structure Calculations with Chemical Accuracy*; Langhoff, S. R., Ed.; Kluwer Academic Publishers: Dordrecht, The Netherlands, 1995; p 357.

(4) Roos, B. O.; Andersson, K.; Fülscher, M. P.; Malmqvist, P.-Å.; Serrano-Andrés, L.; Pierloot, K.; Merchán, M. In *Advances in Chemical Physics: New Methods in Computational Quantum Mechanics*; Prigogine, I., Rice, S. A., Eds.; John Wiley & Sons Inc.: New York, 1996; Vol. XCIII, p 219.

(5) Roos, B. O. *Acc. Chem. Res.* **1999**, *32*, 137−144.

(6) Gonzales-Luque, R.; Garavelli, M.; Bernardi, F.; Merchán, M.; Robb, M. A.; Olivucci, M. *Proc. Natl. Acad. Sci. U.S.A.* **2000**, *97*, 9379−9384.

(7) Ferre, N.; Olivucci, M. *J. Am. Chem. Soc.* **2003**, *125*, 6868−6869.

(8) Robb, M. A.; Garavelli, M.; Olivucci, M.; Bernardi, F. In *Reviews in Computational Chemistry*; Lipkowitz, K. B., Boyd, D. B., Eds.; Wiley-VCH: New York, Chichester, 2000; pp 87−146.

(9) Olivucci, M.; Robb, M. A.; Bernardi, F. In *Conformational Analysis of Molecules in Excited States*; Waluk, J., Ed.; Wiley-VCH: New York, 2000; pp 297−366.

(10) Sinicropi, A.; Pischel, U.; Basosi, R.; Nau, W. M.; Olivucci, M. *Angew. Chem., Int. Ed.* **2000**, *39*, 4582−4586.

(11) Sinicropi, A.; Pogni, R.; Basosi, R.; Robb, M. A.; Gramlich, G.; Nau, W. M.; Olivucci, M. *Angew. Chem., Int. Ed.* **2001**, *40*, 4185−4189.

(12) De Vico, L.; Page, C. S.; Garavelli, M.; Bernardi, F.; Basosi, R.; Olivucci, M. *J. Am. Chem. Soc.* **2002**, *124*, 4124−4134.

(13) Merchan, M.; Serrano-Andrés, L. *J. Am. Chem. Soc.* **2003**, *125*, 8108−8109.

(14) Garavelli, M.; Celani, P.; Bernardi, F.; Robb, M. A.; Olivucci, M. *J. Am. Chem. Soc.* **1997**, *119*, 6891−6901.

(15) Page, C. S.; Olivucci, M. *J. Comput. Chem.* **2002**, *24*, 298−309.

(16) Gross, E. K. U.; Dobson, J. F.; Petersilka, M. In *Density Functional Theory*; Nalewajski, R. F., Ed.; Springer: Heidelberg, 1996.

(17) Casida, M. E. In *Recent Advances in Density Functional Methods*; Chong, D. P., Ed.; World Scientific: Singapore, 1995; Vol. 1, pp 155−193.

(18) Furche, F.; Ahlrichs, R. *J. Chem. Phys.* **2002**, *117*, 7433−7447.

(19) Hsu, C.-P.; Hirata, S.; Head-Gordon, M. *J. Phys. Chem. A* **2001**, *105*, 451−458.

(20) Shao, Y.; Head-Gordon, M.; Krylov, A. I. *J. Chem. Phys.* **2003**, *118*, 4807−4818.

(21) Fantacci, S.; De Angelis, F.; Selloni, A. *J. Am. Chem. Soc.* **2003**, *125*, 4381−4387.

(22) Barone, V.; Fabrizi De Biani, F.; Ruiz, E.; Sieklucka, B. *J. Am. Chem. Soc.* **2001**, *123*, 10742−10743.

(23) Migani, A.; Robb, M. A.; Olivucci, M. *J. Am. Chem. Soc.* **2003**, *125*, 2804−2808.

(24) Vreven, T.; Morokuma, K. *J. Chem. Phys.* **2000**, *113*, 2969−2975.

(25) Sobolewski, A. J.; Domcke, W. *Phys. Chem. Chem. Phys.* **1999**, *1*, 3065−3072.

(26) This structure corresponds to the last optimized point along the S_1 Z → E MEP of **1**.

(27) This structure corresponds to the last planar optimized point along the S_1 Z → E MEP of **1**.

(28) Andersson, K.; Barisz, M.; Bernhardsson, A.; Blomberg, M. R. A.; Cooper, D. L.; Fleig, T.; Fülscher, M. P.; De Graaf, C.; Hess, B. A.; Karlström, G.; Lindh, R.; Malmqvist, P.-Å.; Neogrády, P.; Olsen, J.; Roos, B. O.; Schmmelpfennid, B.; Schültz, M.; Sadlej, A. J.; Schütz, M.; Seijo, L.; Serrano-Andrés, L.; Siegbahn, P. E. M.; Stårling, J.; Thorsteinsson, T.; Veryazov, V.; Widmark, P.-O. *Molcas*, Version 5.1; University of Lund: Sweden, 2000.

(29) Adamo, C.; Barone, V. *Chem. Phys. Lett.* **1999**, *314*, 152−157.

(30) Adamo, C.; Scuseria, G. E.; Barone, V. *J. Chem. Phys.* **1999**, *111*, 2889−2899.

(31) Becke, A. D. *Phys. Rev. A* **1988**, *38*, 3098−3100.

(32) Perdew, J. P.; Wang, Y. *Phys. Rev. B* **1992**, *45*, 13244−13249.

(33) Becke, A. D. *J. Chem. Phys.* **1993**, *98*, 5648−5652.

(34) Slater, J. C. *The Self-Consistent Field for Molecules and Solids*; McGraw-Hill: New York, 1974; Vol. 4.

(35) Vosko, S. H.; Wilk, L.; Nusair, M. *Can. J. Phys.* **1980**, *58*, 1200.

(36) Lee, C. T.; Yang, W. T.; Parr, R. G. *Phys. Rev. B* **1988**, *37*, 785−789.

(37) Miehlich, B.; Savin, A.; Stoll, H.; Preuss, H. *Chem. Phys. Lett.* **1989**, *157*, 200−206.

(38) Perdew, J. P.; Burke, K.; Ernzerhof, M. *Phys. Rev. Lett.* **1996**, *77*, 3865−3868.

(39) Perdew, J. P.; Burke, K.; Ernzerhof, M. *Phys. Rev. Lett.* **1997**, *78*, 1396−1396.

(40) Adamo, C.; Barone, V. *J. Chem. Phys.* **1999**, *110*, 6158−6170.

(41) Frisch, M. J.; Trucks, G. W.; Schlegel, H. B.; Scuseria, G. E.; Robb, M. A.; Cheeseman, J. R.; Zakrzewski, V. G.; Montgomery, J. A., Jr.; Stratmann, R. E.; Burant, J. C.; Dapprich, S.; Millam, J. M.; Daniels, A. D.; Kudin, K. N.; Strain, M. C.; Farkas, O.; Tomasi, J.; Barone, V.; Cossi, M.; Cammi, R.; Mennucci, B.; Pomelli, C.; Adamo, C.; Clifford, S.; Ochterski, J.; Petersson, G. A.; Ayala, P. Y.; Cui, Q.; Morokuma, K.; Malick, D. K.; Rabuck, A. D.; Raghavachari, K.; Foresman, J. B.; Cioslowski, J.; Ortiz, J. V.; Baboul, A. G.; Stefanov, B. B.; Liu, G.; Liashenko, A.; Piskorz, P.; Komaromi, I.; Gomperts, R.; Martin, R. L.; Fox, D. J.; Keith, T.; Al-Laham, M. A.; Peng, C. Y.; Nanayakkara, A.; Gonzalez, C.; Challacombe, M.; Gill, P. M. W.; Johnson, B.; Chen, W.; Wong, M. W.; Andres, J. L.; Gonzalez, C.; Head-Gordon, M.; Replogle, E. S.; Pople, J. A. *Gaussian 98*, Revision A.7; Gaussian Inc., Pittsburgh, PA, 1998.

(42) Stratmann, R. E.; Scuseria, G. E.; Frisch, M. J. *J. Chem. Phys.* **1998**, *109*, 8218−8224.

(43) Cave, R. J.; Burke, K.; Castner, E. W., Jr. *J. Phys. Chem. A* **2002**, *106*, 9294−9305.